Phase equilibria and glass transition in colloidal systems with short-ranged attractive interactions: Application to protein crystallization

Giuseppe Foffi, Gavin D. McCullagh, Aonghus Lawlor, Emanuela Zaccarelli, and Kenneth A. Dawson
Irish Centre for Colloid Science and Biomaterials, Department of Chemistry, University College Dublin, Belfield, Dublin 4, Ireland

Francesco Sciortino and Piero Tartaglia
Dipartimento di Fisica, Istituto Nazionale per la Fisica della Materia, and INFM Center for Statistical Mechanics and Complexity, Università di Roma La Sapienza, Piazzale A. Moro 2, I-00185 Roma, Italy

Davide Pini
Istituto Nazionale per la Fisica della Materia and Dipartimento di Fisica, Università di Milano, Via Celoria 16, 20133 Milano, Italy

George Stell
Department of Chemistry, State University of New York at Stony Brook, Stony Brook, New York 11794-3400

We have studied a model of a complex fluid consisting of particles interacting through a hard-core and short-range attractive potential of both Yukawa and square-well form. Using a hybrid method, including a self-consistent and quite accurate approximation for the liquid integral equation in the case of the Yukawa fluid, perturbation theory to evaluate the crystal free energies, and mode-coupling theory of the glass transition, we determine both the equilibrium phase diagram of the system and the lines of equilibrium between the super-cooled fluid and the glass phases. For these potentials, we study the phase diagrams for different values of the potential range, the ratio of the range of the interaction to the diameter of the repulsive core being the main control parameter. Our arguments are relevant to a variety of systems, from dense colloidal systems with depletion forces, through particle gels, nanoparticle aggregation, and globular protein crystallization.

I. INTRODUCTION

Recently novel results in the statistical mechanics of the fluid state have emerged from a series of studies of the phase diagram of particles with a hard-core and short-ranged attractive potential. At first sight, this type of interaction potential would have been expected to yield the well known phase diagrams of simple solids, liquids and gases. Here we shall see that a different scenario emerges.

In many practical situations attractive forces, which are short ranged compared to the size of the particles, arise because the size of the particles itself is large, whilst the physical forces retain their typical microscopic range. Thus, in order to model large molecules, such as proteins, colloids, and nanoparticles, one often works in a regime where the ratio of the range of attraction to the size of the repulsive core is small. This crucial issue is emerging in the literature in such areas as protein crystallization [1,2], dense colloids [3–6], nanoparticle assemblies, preceramic particle gelation, latex formation, Buckminster fullerenes [7], and many others. In some arenas its relevance begins to be recognized, while in others it still remains to be understood.

Atoms or molecules interacting via a potential with a repulsive core and an attractive tail may form gases, liquids and solids as a function of the temperature and density. The attraction is responsible for the liquid-gas transition, while the solid is dominated by the repulsion. In the low-to-medium range of densities, particle entropy and energy enter the free energy and compete to produce liquid (energy-favored) and gas (entropy-favored) phases. Thus, beneath the

critical point, the total system free energy is optimized if the system splits into two subsystems, and thereby a sum of two independent free energies. One of these free energy terms is dominated by the energy (liquid) and the other (gas) by the entropy. A homogeneous, unseparated system, maintained at the average density of the two subsystems, would not be able to fully optimize either energy or entropy. This, in essence, is the cause of typical first-order phase transitions between a liquid and a gas. In the liquid, as the density increases, the remaining diffusive motions of the particles are reduced and their attendant (configurational) entropy diminishes. Now, the random structure of a liquid is favored provided overall diffusive particle motion is possible. When, at higher densities, diffusion is greatly limited, the free volume is better utilized by making a regular crystalline array, and the entropy of the system is increased by the vibrations of particles within the regular array of a crystal. This is the reason why hard-sphere fluids begin to form a regular crystal at about 49% volume fraction, and above the freezing transition at 55% have a higher entropy than a liquidlike structure at the same volume fraction. Indeed, for hard spheres, at volume fraction between 49% and 55% the system again phase separates to achieve the optimal value of entropy: a lower density fluid of 49% volume fraction and a well-packed crystal at 55%. Nevertheless, it is well known that in some experimental studies the system may be unable to access the crystalline state rapidly enough, and the disordered supercooled liquid structure *freezes* into a glass. For hard-sphere fluids, this occurs at a volume fraction higher than about 58%. The formation of the glass is a signal that equilibrium quantities, such

as the free energy, may not be sufficient to describe the behavior of the system, and that long-lived dynamically arrested states may be important under such conditions.

It is possible to relate these qualitative comments to recent understanding acquired from experiments, simulations, and theory. Thus, there is a separation of time scales in dense systems, including supercooled liquids, in which particles spend a long time trapped by a surrounding cage and thereafter they escape from it. In fact, dynamically slowed systems begin to exhibit a plateau in the self-correlation function, reflecting the time spent in cages, and then a decay (α-relaxation) reflecting escape from the cage and free configurational motion. This approach to the glass transition was formalized [8] with the idea that motions in dense fluids can be divided into intrabasin and interbasin motions, where the basins refer to the multidimensional potential energy as a function of the particles coordinates. This separation of time scales, and thereby type of motion, is reasonable for dense systems, and may be used to justify a conceptual partitioning of the entropy into two parts, a configurational and a local contribution [9]. These ideas can be reexpressed by considering the system, at a fixed average density, composed of central particles trying to escape their cages of neighbors, which are themselves fluctuating and exchanging with their neighbors. Evidently, the α-relaxation process corresponds, in systems very close to arrest, to the escape of the central particles from their cages after some time. In the absence of attractive forces, or for relatively long-ranged ones, the motions of the cage are restricted by the packing forces. This picture is relatively clear, at least in a phenomenological manner, for hard-core spherical particles. For systems that possess a strong repulsion, and a long-ranged attraction, there are no new special features. Thus both "central" and "cage" particles remain in their mutual range of attraction while the structural rearrangement takes place. The resulting cage breaking can be viewed as being almost the same as that for hard spheres, but with changed zero of energy. Even if we acknowledge that there are effects due to attractions, they can still be considered to be weak perturbations of the picture arising from the hard-core spherical particles.

Now let us turn from the scenario just described, typical of hard-sphere particles or particles where the attractions are long-ranged compared to the core size, to situations where attractions play a principal role. In this case, the freedom of the cage particles is considerably reduced. Indeed, particles must remain within a certain distance from each other where substantial attractive energies are still available, or they lose the advantages of being in the liquidlike structure. This being so, the cage around the central particle is much more rigid, since only smaller excursions from average positions of these cage particles are possible. In fact, for sufficiently narrow wells, the time that a particle spends inside the cage increases; a plateau regime results, and the system will eventually freeze. This "cage rigidity" was also the determining factor in hard-core particles at very high density, leading to the typical colloidal "repulsive glass." Here, though the mechanism and detailed laws will be different, we see that short-ranged attractions are able to cause cage rigidity, and formation of a solid, either a glass, or a crystal. Following

these arguments we see that for particles with short-ranged attractions, the density and temperature window over which the liquid state is stable, is greatly reduced since the configurational entropy is reduced. The system separates into a low-density fluid state where there is sufficient free motion, and a dense state where there is, not in any case, sufficient configurational entropy to sustain a liquid, and the system freezes. This state will be a crystal or a dynamically arrested state. Based on the developing views of others, and what we shall present here, all these expectations are borne out from precise calculations and are increasingly found in experiments.

From the above discussion, we may expect that when attractions are short ranged the arrested glass is of different nature than the typical repulsive one, since it is favored by both the energy (because the particles are not close enough to sample mainly repulsive energy), and the local entropy (given that the density is yet relatively low). We have earlier called this arrested state an attractive glass [10,11], and the crystal, previously found by a number of others [12–14], we name the attractive crystal. This distinguishes it from the typical face-centred-cubic (fcc) crystal formed by repulsive forces and the analogous repulsive glassy state.

Given the possibility that for short-ranged attractions, solids—both crystals and glasses—can be formed by these two distinct mechanisms leading to cage rigidity, we may suppose that it is possible, in principle, for them to co-exist. For fixed (short)-ranged potential one way of changing the balance of attraction and repulsion is to change the density, and we comment that such coexistence has been previously shown for crystals [12–14], and glasses [10,11], and is also reproduced here.

In summation, we expect that, as the well width is narrowed, the liquid state becomes progressively less favored, and is replaced by a conventional repulsive crystal or its equivalent glass. An attractive crystal and its equivalent attractive glass should also be present at higher densities, both types of solids coexist at some typical densities where attractions and repulsions compete. From the preceding considerations, we expect that these predictions should be general, irrespective of the detailed shape of the potential, and reflect the typical range of the potential.

We have studied two potential energy models typically used to mimic colloidal interactions, the square well (SW) and the hard-core Yukawa potential, using a variety of techniques of condensed-matter theory. We have determined the phase diagrams calculating the liquid free energy using perturbation theory for the SW and the self-consistent Ornstein-Zernike approximation (SCOZA) for the Yukawa potential. The crystalline free energy has been calculated applying second-order perturbation theory for both potentials. This technique has been applied to short-ranged potentials [14–16], with quite remarkable success in reproducing the crystalline free energy in comparison to Monte Carlo experiments. However, it has been noted [14] that the same method is not so satisfactory in calculating the free energy of the liquid and gas states for very narrow attractive ranges, and this affects the accuracy of the phase diagram [14,17]. To avoid this problem in the case of the Yukawa potential, we have modified the calculation so that the proven good fea-

tures of the perturbation theory of the crystal are combined with the proven quality of the SCOZA for the liquid and gas free energies to produce a phase diagram that is of uniformly good quality. Currently there is no working SCOZA method for the SW case, though there is no fundamental barrier to develop one.

In our work, the ideal mode coupling theory (MCT) [18] of supercooled liquids has been used in order to locate the glass transition curves. For colloids, this method has also been found to describe many elements of the transition to the arrested state [19,20], though it does suffer from some limitations, a matter to which we return later. In the MCT calculations we have used the structure factors from Percus-Yevick approximation (PYA) for the case of SW and from SCOZA for the case of the Yukawa potential. These have proved to be quite accurate theories of the liquid and fluid states. In particular, the SCOZA method has been compared to Monte Carlo simulations for a range of screening parameters ("well widths") of the Yukawa potential, and it has been shown [21,22] that the agreement for the phase diagrams is quantitative, at least for modest values of the screening parameter.

By combining the results from the different methods described above, we are able to give, for some regimes, what we believe to be quite accurate phase diagrams. For the general case we believe that the results are at least qualitatively correct, and provide us a coherent picture of the connection between the well width and the arrangement of gas, liquid, crystal, and glass phases. It is this overview of how the various phenomena fit together that is currently missing, and that should prove useful in the various applications alluded to above. We also point out that, from experiments, it has become clear that the interaction between globular proteins, in the range where they may crystallize, is characterized by short-range attractions [1]. In the case of proteins, a better comprehension of the phenomena would imply the study of anisotropic types of potential [23], due to hydrophilic-hydrophobic patching of the protein surface. The usual approach is, however, to use an effective isotropic interaction obtained by averaging over the anisotropy. Thus, as discussed later, most of our conclusions will be also important to understand the process of protein crystallization.

The paper is organized as follows. In Sec. II we describe the approximate closures to the Ornstein-Zernike liquid integral equation that we have used for the Yukawa and SW potentials. The methods employed to determine the equilibrium fluid and solid phases are described in Secs. III and IV. Section V is devoted to a brief sketch of MCT applied to attractive potentials, while in Sec. VI the relevance of the spinodal curve for colloidal systems is discussed. The complete phase diagram, including the structural arrest lines is discussed in Sec. VII, while Sec. VIII is devoted to our conclusions.

II. APPROXIMATIONS TO THE OZ EQUATION FOR THE YUKAWA AND SQUARE WELL MODELS

In this section we shall discuss the theory used in the investigation of the phase diagram. The Ornstein-Zernike

(OZ) equation for the pair correlation function $h(r)$ is

$$h(r) = c(r) + \rho \int d\mathbf{r}' c(|\mathbf{r} - \mathbf{r}'|) h(|\mathbf{r}'|), \quad (1)$$

where $g(r) = h(r) + 1$ is the radial distribution function and $c(r)$ the direct correlation function. Another important quantity is the static structure factor S_q, which is the equal time correlation function of the density variables in wave vector space

$$S_q = \langle \rho_{-q}(t) \rho_q(t) \rangle / N, \quad (2)$$

where the average $\langle \cdots \rangle$ is performed at equilibrium and the density variables are $\rho_q(t) = \Sigma_i e^{i\mathbf{q} \cdot \mathbf{r}_i(t)}$, where the sum runs over all N particles in the system. The Fourier transform of the correlation function h_q is related to this quantity by the relation $S_q = 1 + \rho h_q$. The OZ relation in the wave vector space reads

$$S_q = \frac{1}{1 - \rho \hat{c}_q}, \quad (3)$$

$\hat{c}_q$ being the Fourier transform of the direct correlation function.

As it stands, Eq. (1) is not closed and some type of approximation is needed in order to solve it. In what follows we have chosen to calculate structural and thermodynamical properties using the PYA for the SW potential and the SCOZA [21,22,24] for the Yukawa potential. Both these model potentials possess some fundamental properties that make them good candidates for studying the properties of attractive colloidal particles when the range of interaction is short. The use of SCOZA has been justified by the success of such approach in predicting simulation data.

A. The SCOZA for the Yukawa potential

The application of SCOZA to a hard-core Yukawa fluid provides a semianalytic calculation of the thermodynamic properties of the fluid, liquid, and gas states of the system [21,22]. SCOZA has been applied to Yukawa systems with relatively large values of the range of the potential, with a satisfactory reproduction of the liquid-vapor binodal curves and a good description of the critical point region.

The hard-core Yukawa fluid is described by the following interparticle potential:

$$v(r) = \begin{cases} \infty, & r < \sigma \\ -\sigma\epsilon \dfrac{e^{-b(r-\sigma)}}{r}, & r \geq \sigma. \end{cases} \quad (4)$$

The parameter ϵ defines the energy scale, while the parameter b, known as screening parameter, determines the range of the potential. The larger the b, the shorter is the range of the potential. In this paper, we set $\sigma = 1$ and $\epsilon = 1$, therefore the screening parameter is in units of the reciprocal of the hard-core diameter, and the temperature in units of the well depth.

SCOZA provides a closure relation for the OZ Eq. (1) by expressing the direct correlation function $c(r)$ in terms of the potential $v(r)$, as for other approximations such as the mean spherical approximation (MSA), PYA, hypernetted chain (HNC) approximation, etc., but introducing one or more state dependent parameters that can be adjusted to force the system to satisfy various exact thermodynamic relations of the system. In particular, the simplest SCOZA studied so far assumes

$$g(r) = 0, \quad r \leqslant \sigma, \tag{5}$$

while $c(r)$ for $r \geqslant \sigma$ is composed of two contributions, describing, respectively, the soft part of the potential and the hard core, as

$$c(r) = -A\beta v(r) + K_{HS} \frac{e^{-b_{HS}(r-\sigma)}}{r} \quad r \geqslant \sigma. \tag{6}$$

The Yukawa function in Eq. (6) takes into account the contribution to $c(r)$ arising from the hard-core repulsion. Thus, the two parameters K_{HS} and b_{HS} can be determined by setting $v(r) = 0$ in Eq. (6) and requiring that both the compressibility and the virial route to thermodynamics lead to the Carnahan-Starling equation of state for a hard-sphere fluid [25]. This amounts to describing the hard-sphere correlations via the Waisman parametrization [26]. The soft part of the contribution in Eq. (6) is assumed to be proportional to $v(r)$ and hence it has the same range of the potential. The proportionality constant A is calculated by imposing the condition that the compressibility and the energy routes yield the same result. This corresponds to the condition [22]

$$-\frac{\partial}{\partial \beta} \hat{c}(q=0) = \frac{\partial^2}{\partial \rho^2} \left(\frac{U^{ex}}{V} \right)_T, \tag{7}$$

where U^{ex} is the excess internal energy [27]. Equation (7) implies a partial differential equation (PDE) for $A(\rho,\beta)$. The Yukawa potential (4) lends itself particularly well to the SCOZA scheme, because, for this kind of interaction, it is possible by means of Eqs. (5) and (6) to establish an analytic relation between $\hat{c}(q=0)$ and U^{ex}, which allows us to obtain straightforwardly a closed PDE from Eq. (7) by using U^{ex} as the unknown quantity instead of $A(\rho,\beta)$ [21,24]. Once the internal energy has been obtained by numerical solution of this PDE, the Helmholtz free energy is calculated by integration with respect to β.

The reasons that led us to adopt SCOZA can be summarized as follows. The method uses a reasonable choice of functional relationship between $c(r)$ and $v(r)$ on the basis of numerous calculations obtained over a number of years. Furthermore, it has been shown [22] that the results obtained are in excellent agreement with computer simulations, at least for not too narrow ranges of the potential. In this sense, it may be viewed as the best semianalytical method to study the Yukawa potential. Finally, it is simple and convenient to obtain numerical solutions of Eq. (7), and this is helpful to make a survey of a problem in a large parameter window, rather than just in a small part of the parameter space. To
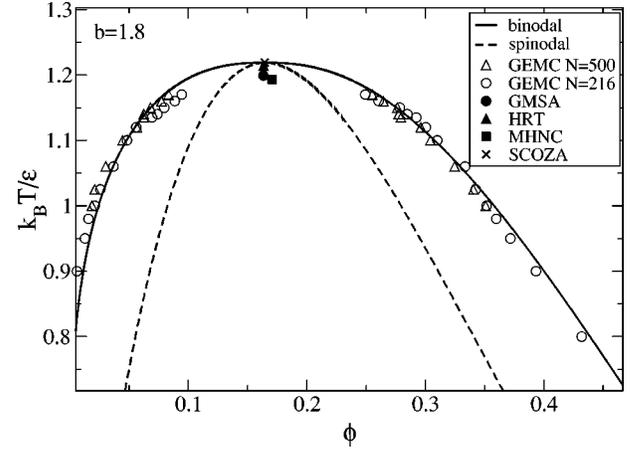

FIG. 1. Liquid-liquid phase diagram from SCOZA compared to simulation data for $b=1.8$. The GEMC data are taken from Shukla [28] (see text for details). The estimation of the critical points are from GMSA, HNC, and HRT.

give the reader some sense of the accuracy of SCOZA in some of the regimes we will discuss later. We present in Figs. 1 and 2 the phase diagrams for $b=1.8$ and $b=6$ calculated using SCOZA, compared with Gibbs ensemble Monte Carlo (GEMC) studies [16,28]. The data by Shukla are the largest system sizes with this potential yet to be studied by GEMC. In all cases, the agreement with SCOZA is excellent, and we may, in this regime of b values and in calculating the phase diagrams, consider SCOZA to be equal to the best simulations. The method is superior to the other simple closures, including, for example, MSA.

Having said this, we note that there is little real information available about the detailed reliability of the closure relation where the potential becomes much narrower than for $b=9$, though it is reasonable to suppose that many properties are still satisfactory for somewhat larger b values. Another comment we may make is that, when the range of the potential narrows, Eq. (6) may not be the optimal closure to ensure that $c(r)$ is accurate. Both these points should be regarded as
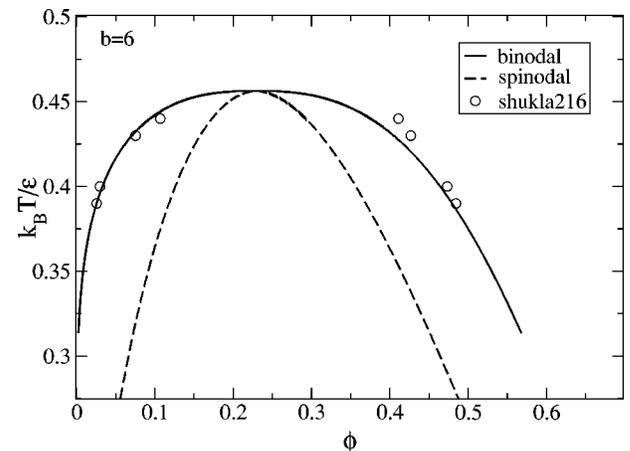

FIG. 2. Liquid-liquid phase diagram from SCOZA compared to simulation data for $b=6$. The GEMC data are taken from Shukla for $N=216$ [28] (see text for details).

words of caution and as potential directions to develop the SCOZA method to better represent the structure in such problems. Indeed this will be the subject of future work.

B. The Percus-Yevick closure for the SW potential

We shall now briefly discuss the closure for a fluid of colloidal particles interacting via a square well potential

$$v(r) = \begin{cases} \infty, & r < \sigma \\ -\epsilon, & \sigma < r < \sigma + \delta \\ 0, & \sigma + \delta < r, \end{cases} \tag{8}$$

where, in the present discussion, we set $\epsilon = \sigma = 1$ and we define the square-well parameter $\Delta = \delta/(\sigma + \delta)$, which parametrizes the attractive range of the potential. This model has been already the object of great interest in colloidal science [29,10]. The state of the system is specified by three control parameters, the packing fraction $\phi = \pi \rho \sigma^3 / 6$ (where ρ is the number density, i.e., $\rho = N/V$), the temperature $k_B T$, and the square-well parameter Δ of the attractive shell.

The PYA for $c(r)$ is $g(r) = 0$ for $r < \sigma$ and

$$c(r) = g(r)[1 - e^{\beta v(r)}] \tag{9}$$

outside the hard core [30]. We solve the OZ equation in PYA using Baxter's method of the Wiener-Hopf factorization [27,31]. This corresponds to rewriting Eq. (1) in terms of the real factor function $Q(r)$, defined for $r > 0$. For $0 \le r \le R$, R being the range of the potential ($\sigma + \delta$ in the present case), one has

$$rc(r) = -Q'(r) + 2\pi \rho \int_r^R ds Q'(s) Q(s - r) \tag{10}$$

as well as, for $r > 0$,

$$rh(r) = -Q'(r) + 2\pi \rho \int_0^R ds (r - s) h(|r - s|) Q(s). \tag{11}$$

$Q(r)$ determines S_q via its Fourier transform

$$S_q^{-1} = \hat{Q}(q) \hat{Q}(q)^*, \tag{12}$$

$$\hat{Q}(q) = 1 - 2\pi \rho \int_0^\infty dr e^{iqr} Q(r). \tag{13}$$

The resulting equations, obtained implementing the PYA in Eqs. (10) and (11), are then solved numerically to calculate the structure factor S_q (see Ref. [10] for more details).

III. THE PERTURBATION THEORY APPLIED TO SOLID AND FLUID PHASES

A. The crystal phase

In this section we shall discuss the method used to calculate the solid free energy. The perturbative approach has previously been used by Gast *et al.* [15] to construct the phase diagram of a colloidal solution with depletion interactions.

Further applications of the method appear in Refs. [14,16]. For example, in [14] the authors compared the results obtained for both phase diagrams and free energies of the solid and liquid phases for an Asakura-Oosawa potential and made comparisons to Monte Carlo calculations. They noted that the phase diagrams are overall reasonably satisfactory, but that the crystal free energies are excellent, in most regimes being essentially quantitative. It was concluded that the potential limitations in accuracy of the phase diagrams arise from the use of perturbation theory to the fluid and liquid phases, rather than the crystal. Also, for the crystal free energies there does not appear to be a significant loss of accuracy when the range of the potential becomes narrow. We have, therefore, applied perturbation theory to the crystal state of the Yukawa potential. Is opportune to note that there are other perturbative approaches in the literature, such as in [29].

The method is summarized as follows. We separate out explicitly the interaction potential as a hard-core contribution plus the attractive tail. The hard-core part of the potential is used as a reference for the perturbation, and the attractive tail is the perturbation itself [27]. In other words, we decompose the potential as

$$v(r) = v_0(r) + v_{att}(r), \tag{14}$$

where $v_0(r)$ is the hard-core repulsive potential and expand around the reference state $v_0(r)$. With this choice, the zeroth-order term of the free-energy expansion coincides with the hard-sphere free energy. Once the perturbation expansion is carried out to second order we have for the Helmholtz free energy the following expression [27]:

$$\frac{\beta F}{N} = \frac{\beta F_0}{N} + \frac{\beta \rho}{2} \int v_{att}(r) g_0(r) d\mathbf{r} + \frac{\beta F_2}{N}. \tag{15}$$

Here $\beta F_2 / N$ is the second-order perturbation term. F_0 and g_0 are, respectively, the Helmholtz free energy and the radial distribution for the reference hard-sphere system.

We focus our attention on the second-order term in the expansion in Eq. (15). Indeed, its exact evaluation requires the calculation of higher-order distribution functions [27], which are very hard to compute or to approximate reasonably. Barker and Henderson [32] proposed an approximation to F_2, based on the following observation. Since

$$\frac{\beta F_2}{N} = -\frac{1}{2} \beta (\langle W_N^2 \rangle_0 - \langle W_N \rangle_0^2), \tag{16}$$

where $W_N = \Sigma_{i<j}^N v_{att}(|\mathbf{r}_i - \mathbf{r}_j|)$, Barker and Henderson proposed to divide the space into concentric spherical shells to calculate averaged properties using the number of particles in each shell. Following this route, they rewrote Eq. (16) in terms of average numbers in the shells

$$\frac{\beta F_2}{N} = -\frac{1}{2} \beta \sum_{ij} (\langle N_i N_j \rangle - \langle N_i \rangle \langle N_j \rangle) v^i v^j, \tag{17}$$

where N_i is the number of particles in the shell i and v_i is the perturbation energy, considered constant, within the shell. The first approximation consists of ignoring the correlations between shells, i.e.,

$$\langle N_i N_j \rangle - \langle N_i \rangle \langle N_j \rangle = 0 \qquad (18)$$

for $i \neq j$. Moreover, inside a given shell, a second approximation is made,

$$\langle N_i^2 \rangle - \langle N_i \rangle^2 \approx \langle N_i \rangle k_B T (\partial \rho / \partial P). \qquad (19)$$

The two approximations (18) and (19) are equivalent to considering the volume of the shells to have the compressibility properties of a macroscopic portion of space (for more details see [32]). As a result, Barker and Henderson approximated the second-order term in the expansion as

$$\frac{\beta F_2}{N} = -\frac{\beta \rho}{4} \left(\frac{\partial \rho}{\partial P} \right)_0 \int v_{att}^2(r) g_0(r) d\mathbf{r}. \qquad (20)$$

This approximation was found to be satisfactory in all calculations carried out so far. In our work the integrals in Eqs. (15) and (20) have been performed by a five-point integration rule, while for differentiation a central-difference scheme has been used [33].

To carry out the calculation, we require the Helmholtz free energy and radial distribution function of the unperturbed hard-sphere system in the solid phase. It has been shown by computer simulation that a hard-sphere fluid shows a solid-fluid transition, for which the fluid phase alone exists up to a packing fraction $\phi = 0.49$ and the solid fcc phases exists for $\phi > 0.55$ [34]. In between, there is a two-phase coexistence of solid and fluid. These properties are well studied and the information required in perturbation theory can be deduced from these studies. We note in passing that recently a renewed interest has been shown in the equilibrium structure of a hard-sphere crystal. Indeed it has been believed for a long time that hard spheres crystallize with an fcc structure. Confocal microscopy observations, however, have rather found a random hexagonal phase which consists of a stack of fcc and hexagonal close packing (hcp) layers [35]. Simulation seems to explain the phenomenon in terms of the small free-energy difference between fcc and hcp structures [36]. In this paper, we assume the crystal equilibrium structure to be fcc since this is believed to be more stable [37].

To provide continuity with previous authors we make the choices described below. The state equation for a hard-sphere fcc solid has been proposed by Hall [38] who derived a phenomenological expression based on computer simulation results, i.e.,

$$Z_{HS} = \frac{P_{HS} V}{N k_B T} \qquad (21)$$

$$= \frac{1 + \phi + \phi^2 - 0.67825 \phi^3 - \phi^4 - 0.5 \phi^5 - 6.028 \phi^6 f(\phi)}{1 - 3\phi + 3\phi^2 - 1.004305 \phi^3} \qquad (22)$$

with $f(\phi) = \exp((\pi \sqrt{2}/6 - \phi)[7.9 - 3.9(\pi \sqrt{2}/6 - \phi)])$. The compressibility can be derived by differentiating the compressibility factor Z_{HS} as

$$\left(\frac{\partial \rho}{\partial p} \right)_0 = \frac{\beta}{Z_{HS} + \phi(\partial Z_{HS}/\partial \phi)}. \qquad (23)$$

In order to calculate the excess hard-sphere Helmholtz free energy F_0^{ex} from the compressibility factor Z_{HS}, a thermodynamic integration in the packing fraction ϕ can be performed, obtaining

$$\frac{\beta F_0^{ex}}{N}(\phi) = \frac{\beta F_0^{ex}}{N}(\phi^*) + \int_{\phi^*}^{\phi} (Z_{HS} - 1) \frac{d\eta'}{\eta'}. \qquad (24)$$

Since the zero-density limit of a fcc crystal cannot be represented as easily as the one for a gas, alternative routes to perform the thermodynamic integration in Eq. (24) have to be devised [34]. We have chosen to perform the integration starting from a packing fraction value of $\phi^* = 0.544\,993$, for which the value of the free energy has been calculated by computer simulation to be $F_0^{ex}(\phi^*)N = 5.918\,89$ [39]. We recall that the excess Helmholtz free energy is defined as the excess with respect to the ideal gas contribution [27].

For the radial distribution function $g_0(r)$, we have used an analytic formulation proposed by Kincaid and Weis that fits Monte Carlo simulation for a hard-sphere fcc solid [40]. This formulation is known to provide a good estimate of the hard-sphere radial distribution function, at least in the range $0.52 \leq \phi \leq 0.565\,18$. Equations (15) and (20) can now be solved.

Once the Helmholtz free energy is evaluated, following the route we have just described, the Gibbs free energy and the pressure can be calculated as

$$\beta G = \frac{\partial(\rho \beta F)}{\partial \rho}, \qquad (25)$$

$$\beta P = \frac{\rho \beta G}{N} - \frac{\rho \beta F}{N}. \qquad (26)$$

We have earlier noted that the perturbation theory for the crystal is highly accurate. Indeed, the second-order perturbation term is useful, but it is interesting to note that the great bulk of the free energy correction for narrow well problems is captured by the first-order term alone. To understand this, it is worth reflecting on the fact that the free energy of the crystal in the presence of short-ranged attractions is referred to the hard-core crystal, and there is no question of the perturbation theory having to determine *a priori* any gross structural information. The corrections from attractions arise by virtue of the small changes in local vibrations that the particles make around their lattice positions, a portion of these motions involving the particles being within their mutual attractive range. In first-order perturbation theory, these contributions are treated as if the nature and distribution of the vibrations is unchanged, and the additional attractive energy contributions calculated essentially as an integral over the

attractive potential multiplied by the zeroth-order hard-core correlation function. The fact that second-order contributions are typically small is suggestive. In a heuristic manner, we may argue that the intrinsic limitation on the extent and complexity of the phase space of the localized particles, imposed by their being in a crystalline state, means that even when attraction is incorporated, the changes in the nature and distributions of these vibrations are small. We note that this rationale is clearly inapplicable to the case of liquid, gas, and fluid states, where the addition of attractions significantly affects the distribution of particles motions. Possibly this is the reason why perturbation theory works well for the crystal, indeed far outside its expected limitations, but is less successful for the other states. For completeness we note that for the crystal (Yukawa and SW) the errors, as estimated by the ratio of second-order to first-order terms are typically of order 0.5%. For the liquid they can be larger. We have, however, also studied a square-well fluid using perturbation theory, and used these results along with those for the crystal to generate a phase diagram. The perturbation theory of the square-well fluid is, therefore, briefly discussed below.

B. Liquid phase for the SW fluid

In this section we shall discuss the method we adopted to calculate the thermodynamical properties of a fluid of colloidal particles interacting via a SW potential.

We chose the hard-sphere fluid as the reference system and treated the attractive part as the perturbation. The natural choice to describe the thermodynamics of a hard-sphere fluid is the Carnahan-Starling (CS) equation of state [25]

$$\frac{\beta P}{\rho} = \frac{1 + \eta + \eta^2 - \eta^3}{(1 - \eta)^3}. \tag{27}$$

The CS equation provides an accurate account of the thermodynamic behavior of the hard-sphere fluid for the entire region of the fluid phase. Its very simple analytical form makes it possible to obtain a closed expression for the Helmholtz free energy by integrating over density, as in Eq. (24). The zero-density limit of the free energy is the ideal gas value, so the thermodynamic integration starts from zero density. Thus, we obtain

$$\frac{\beta F^{ex}}{N} = \frac{\eta(4 - 3\eta)}{(1 - \eta)^2}. \tag{28}$$

The compressibility is evaluated as in Eq. (23) by differentiation. For the radial distribution function we use a modification of the analytical PYA $g_0(r)$ for a hard-sphere fluid that was proposed by Verlet and Weis [41] to overcome certain limitations of this closure. Indeed, in PYA [30], the contact value $g_0(r = \sigma)$ of the radial distribution function underestimates the real value obtained by computer simulation and, also, the oscillations of the tail are slightly out of phase and too weakly damped. Verlet and Weis proposed

$$g_0(r/\sigma, \phi) = g_0'(r/\sigma', \phi') + \delta g_1(r). \tag{29}$$

Here, $g(r)$ is written as the sum of two terms. The first term corresponds to the solution for $g_0(r)$ within PYA, but evaluated at a smaller packing fraction value ϕ' and a smaller diameter σ', while the second term is a short-ranged correction $\delta g_1(r)$. The parameter σ' is then evaluated via a minimization of the difference between the simulation result for $g_0(r)$ and the PYA analytical result, between 1.6σ and 3σ. This contribution improves the long-range behavior of the PYA result. The addition of the short-range term $\delta g_1(r)$ improves the value at $r = \sigma$. Analytical forms for ϕ' and $\delta g_1(r)$ are given by the authors of Ref. [41]. The improved radial distribution is within 1% of the computer simulation result in the whole range of packing fractions. With this result, the Helmholtz free energy for the hard-sphere reference system is calculated, and we may then proceed as we did in the preceding section to calculate the Gibbs free energy G and pressure P using Eqs. (25) and (26).

IV. THE CONSTRUCTION OF PHASE DIAGRAM OF THE YUKAWA MODEL BY A HYBRID METHOD

In the case of the Yukawa potential we have modified the approach of previous researchers somewhat in order to obtain the benefits of the best methods of condensed and liquid state theory. We have used SCOZA to calculate the liquid, gas, and fluid phases free energy, but applied perturbation theory for the crystal free energy. To mark the difference with previous calculations, where phase equilibrium lines had been calculated by perturbation theory both for the crystal and for the fluid phase, we name our approach a hybrid method.

Phase boundaries between two phases (gas-liquid, fluid-solid, etc.) are obtained by imposing the standard conditions

$$\mu^{(1)} = \mu^{(2)}, \tag{30}$$

$$P^{(1)} = P^{(2)}, \tag{31}$$

where μ is the chemical potential, i.e., the Gibbs free energy per particle, $\mu = G/N$.

In those cases where SCOZA and perturbation theory are quantitatively validated, the equilibrium phase diagram is highly accurate. As noted above, and shown in Figs. 1 and 2, the SCOZA is well validated up to values of $b = 9$. For values of b less than or equal to 6, results are indistinguishable in terms of phase equilibria from the best simulations that have been carried out [22,16,28]. Similarly, as we shall discuss later, the perturbation theory rarely produces an error of more than 0.5% in the free energy of the solid phase, although this analysis is based on certain assumptions about the perturbation series. Combining these observations, we believe that our phase diagrams are quantitatively accurate up to at least $b = 9$. Beyond that, we make no particular claim, except that we expect that this hybrid method should still remain superior to the typical theoretical approximations that have been applied previously. Simulations have not been carried out beyond $b = 9$.

V. GLASS TRANSITION AND MODE COUPLING THEORY

A. Theory

The study of the glass transition in colloidal systems has been one of the most striking cases of verification of the current theories of supercooled liquids. Early experimental studies [42,43] involved colloidal particles that are very closely represented by hard spheres where only excluded volume effects are important at high concentrations. Moreover, in contrast to simple atomic liquids, it is possible to avoid the crystalline phase beyond volume fractions of 49% for sufficiently long periods of time to study the glassy-type dynamical processes, and ultimately the colloidal glass. The agreement between certain aspects of MCT and experiments on colloids is quite satisfactory [44] and the details of the time correlation functions are quite well reproduced. It is widely believed that, in deeply supercooled molecular liquids, the slow dynamics involves more complex dynamical processes than those described by MCT, and there the theory becomes of more qualitative applicability. Thus, the case of colloidal particles is of some practical interest in applying this type of theory.

In fact, even for colloids, small discrepancies appear in the comparison between experiments and MCT. The most important is the value of the critical volume fraction for the hard-sphere arrest transition, the experimental value being about 58%, while MCT predicts about 52%. This is of little importance where the dynamical laws at the hard-sphere transition are being compared between the experiment and theory. Previous researchers have applied a shift to the transition volume fraction, and then fitted the laws in this region [43]. Since the only current information on arrest driven by attractive interactions is that provided by MCT [10], there is as yet no accepted manner in which we can correct the MCT curves. This is somewhat inconvenient in the current context, since for some parts of the parameter space the equilibrium phase diagrams are quantitatively accurate, and it would be very satisfying to be able to superimpose, without correction, the relevant MCT arrest curves.

We now briefly review the nature of MCT, and discuss the type of information it yields. The MCT of supercooled liquids describes the nonergodicity transition by a nonlinear integrodifferential system of equations for the normalized time correlation functions of density fluctuations $\Phi(q,t)$. Apart from parameters entering from the microscopic motion, the only input to the MCT equations is the equilibrium wave-vector-dependent structure factor of the system, S_q. The glass transition lines can be identified by studying the long-time limit of the MCT equations, which determine the nonergodicity parameter of the system $f_q = \lim_{t\to\infty} \Phi(q,t)$. An ergodic state is characterized by $f_q = 0$. This value is always a solution of the MCT long-time limit equations [18]. Thus, the glass transition appears as an ergodic to nonergodic transition for the system, where $f_q \neq 0$ solutions arise. These points, thus, correspond to bifurcation singularities of the MCT equations, and, depending on the number of control parameters of the model, these can be of increasingly higher order, producing interesting features of the arrested states diagrams.

A good quality S_q is an important input for a good description of the MCT arrest transition, as for the equilibrium phase diagram. In the earliest discussions of colloidal systems with short-ranged attractive interactions, the Baxter interaction [45,46], a limiting case with an infinitely deep and zero-ranged SW attractive potential, was discussed by a number of authors [20,47,48]. Subsequent studies indicated that the MCT equations are pathological for this interaction [49]. The calculations were, therefore, extended to a SW potential both in the PYA and the MSA [10]. Another solution of the MCT equations was obtained using the Yukawa potential and the MSA [19]. Some common aspects emerged in these works. However, the SW model at first appeared to give a richer behavior for the arrest transition curve. Thus, the system was shown to possess a glass transition curve in the parameter plane $(\phi, k_B T)$; the shape of this curve depends on the value of the SW parameter Δ [10]. For narrow well widths, two branches of the glass curve have been identified. These have been interpreted, respectively, as transition between a fluid phase and repulsion dominated glass (this is the typical repulsive glass) and between a liquid and an attractive-interaction dominated glass (named the attractive glass). The two branches join and for $\Delta \leq 4.11\%$, a glass-glass coexistence between the two different types of glass appears. This coexistence line terminates in an end point, beyond which the nonergodicity parameters become the same for the two types of structures. The relevant singularity points, such as the end point or the point where the glass-glass transition line reduces to a single point, are identified with higher-order singularities of MCT equations and lead to unusual logarithmic dynamical relaxation laws [10,18]. The mechanical properties of the system have been also studied [11] and they reinforce this interpretation. Earlier studies of the Yukawa potential did not locate this glass-glass phenomenon [19], but it was subsequently realized that the screening parameters, which had been studied, were not large enough [50], and further calculations seem to give clear indications that both the SW and Yukawa potentials give the same typical behavior [51], implying that this does not crucially depend either on the potential shape or on the approximation used for calculating the structure factor. Thus, it is now believed that this glass-glass scenario and the attendant dynamical laws, are essentially a universal feature of the very short-ranged attractive potential.

We note in passing that the formation of two solid glass phases for very short-ranged potentials should not be too surprising. In fact we have earlier alluded to the fact that there are two crystalline phases in the phase diagram of such potentials. We may typically view glasses or arrested states as long-lived metastable states of the system that have not been able to equilibrate to the nearby crystal and which are trapped in a restricted portion of phase space. In this sense we may expect each crystal to have associated to it a particular glass type. Since one of the crystals in our phase diagram is ''attractive energy dominated'' and the other ''repulsive energy dominated,'' it is hardly surprising that there should be two types of glass, dominated by the two regimes of interaction.

A further comment on the relevance of these glass curves is that we may see them as more than simply "transition curves." If we reflect more deeply on the nature of the equilibrium phase diagram and the thermodynamic states present in them, we recognize that at a deeper level they are reflecting the fact that for those particular parameters, the phase space is dominated by a particular structure: a crystalline, liquid, or gas structure. The arrest curves carry analogous information. Thus, in the vicinity of the arrest curve, we may understand that most of phase space is becoming increasingly inaccessible and breaks into smaller regions that are disconnected. That this may occur even for states that appear to have static structures typical of liquids is the distinguishing feature of glasses. Associated to this observation is the dynamical slowing and tendency to arrest during any phase separation through which such a glass curve passes. We shall argue in the conclusions that such phenomena are relevant in protein crystallization.

B. Experimental studies

We now discuss some of the particular experimentally determined features that are associated with dynamical arrest driven by attractive interactions. For example, Verduin and Dhont [4] determined a curve of structurally arrested states in the phase diagram of a system with short-ranged attractive depletion interactions. This locus, in some cases, intersects the binodal line and is referred to as transient gelation when observed in the spinodal region. The authors of Ref. [4] were the first to comment that MCT might also be applicable to cases where attractive interactions are important. As we noted above, subsequent results of such calculations have been most interesting [10,11,19]. In addition a number of other experimental programs involving particles with depletion interactions have been published which offer many interesting insights for example in [52,53]. In particular, Poon and co-workers [5] have studied the arrest transition for systems where the range of the interactions is short, and their more recent work on this topic involves detailed connection to the theory described above [54]. Other systems may have certain advantages over the depletion interaction system, but it is as yet too early to decide this issue [6,55–60]. The results are typically quite promising, with some of these other systems also exhibiting some of the phenomena predicted by the theory. We may note in particular a more recent set of experiments that are intriguing in that they make detailed predictions for the correlation functions in a particular (reentrant) part of the phase diagram. Thus, concentration time correlation functions have been observed in a polymer micelle system with a decay process much longer than the usual stretched exponential, and the results have been well fitted to a logarithmic time relaxation [61] as predicted by the theory [62].

The development of experimental understanding, and deepening of the theory of systems with short-ranged potentials is really just beginning, and many experimental programs have now been commenced or reoriented to make progress. However, early information indicates that the MCT-type theory may be able to describe main elements of the principal phenomena, at least for reasonably high volume fractions, where it is possible to separate aging from dynamical arrest in a reasonably clean manner.

VI. ARE SPINODALS IN COLLOIDAL SYSTEMS MEANINGFUL?

Here we will take the liberty of raising a few issues in relation to spinodal curves that are calculated via SCOZA, or indeed many other typical liquid state theories. The reason that we make these comments is that such curves should have a particular status for these colloidal systems that are not relevant generally for molecular systems. We note first that the spinodal curve is determined from the condition that the curvature of the free energy with respect to the relevant density variable becomes zero, and that this corresponds to the fluid phase becoming unstable as we lower the temperature. Between the binodal and the spinodal, the liquid and gas states in coexistence may be the global free-energy minima, but the fluid state remains metastable. Inside the region bounded by the spinodal, only the liquid and gas states in coexistence are stable. Now it is well known [63] that the free energy is a convex function, and it possesses only one minimum, and for some years now it has been understood that the spinodal curve determined from approximate theories (e.g., mean-field theories) that consider two separate branches of the free energy and then connect them, has no real scientific basis. Careful Monte Carlo simulations carried out in systems of increasing size [64] have lead to the conclusion that the spinodal curve shifts with the system size, merging with the binodal in the limit of infinite systems. There is some loosely defined kinetic phenomenon however [64,65], though even there it is not possible to define a spinodal curve, but a cross-over regime where the kinetic mechanisms begin to change from nucleation and growth to more collective phenomena. Interestingly enough, when the particle size becomes large, these more sophisticated expectations are less relevant. Thus, it transpires that the relevant parameter in this story is the ratio of the particle diameter to the correlation length of the fluid. For very large particles, such as high molecular weight polymers, colloidal and other particles, the microscopic length is so large that one has to be extremely close to the critical point to see fully developed fluctuations beyond the mean-field type ideas. Another consequence of this is that critical exponents in such systems as proteins [66] and micelles [67] have often been measured with mean-field values because experiments were not performed in the true critical regime. Similarly, the normal scepticism about the existence of a spinodal curve should be less relevant here, and we may expect the colloidal systems to exhibit quite reasonable spinodal behavior. We have, therefore, included the spinodal curve in our phase diagrams.

In concluding this section on dynamically defined objects in the phase diagrams, it is commented that we have chosen to plot the MCT curves through the metastable regions between binodals and spinodals. Again, in colloidal systems, for the reasons given above, it is to be expected that such curves would have meaning, whereas they would not be meaningful in molecular systems.
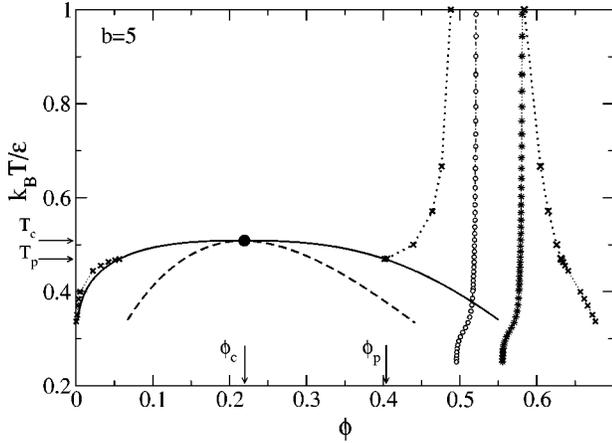
FIG. 3. Phase diagram for the Yukawa fluid with screening parameter $b=5.0$. The crosses represent the fluid-solid phase transition, the continuous line is the binodal, and the dashed one is the spinodal. The filled circle is the critical point. The glass transition line as evaluated for mode coupling theory is also displayed (open circles). The glass line shifted to obtain the asymptotic value for $T \to \infty$ to be the experimental packing fraction $\phi=0.58$ is presented (stars). The subscripts c and p refer to the critical point and the triple point, respectively.

VII. PHASE EQUILIBRIA AND DYNAMICAL ARREST LINES

In this section we combine the results from the different techniques described above to exhibit the state of the system for given well depth.

A. Yukawa potential

In this section results for the Yukawa potential with the temperature in units of the well depth ($k_B T/\epsilon$) plotted against the volume fraction of the system ϕ are presented. The values of the well width are determined via the screening parameter of the Yukawa b. The hard-core radius is fixed at unity, so all quoted lengths are in units of the hard-core
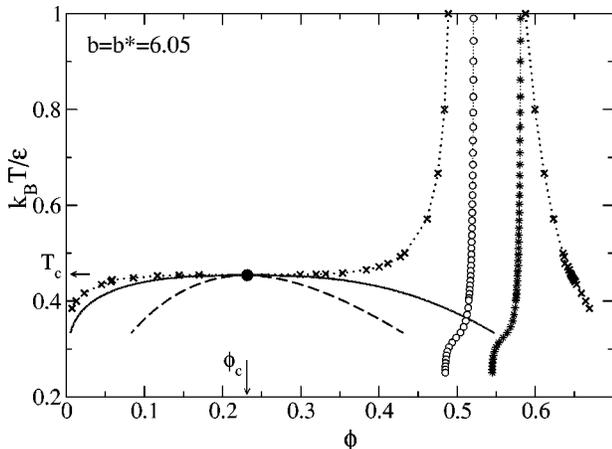

FIG. 4. As in Fig. 3 with $b=6.05$. The fluid branch of the fluid-crystal coexistence line now passes through the liquid-gas critical point.
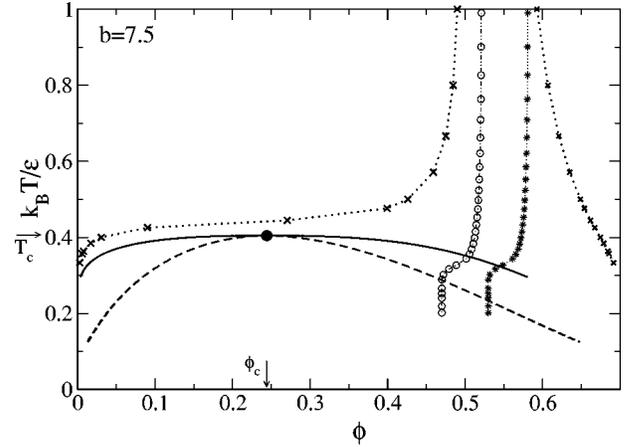

FIG. 5. As in Fig. 3 with $b=7.5$.

diameter. We show results for values of $b=5$ (Fig. 3), $b=6.05$ (Fig. 4), $b=7.5$ (Fig. 5), $b=30$ (Fig. 6), $b=60$ (Fig. 7), and $b=100$ (Fig. 8). For comparison we also show (Fig. 9) a calculation for the square well system with $\Delta=0.03$.

We begin with the largest well width, corresponding to $b=5$, see Fig. 3. Here the well width, considered say as the distance of half-amplitude of a Yukawa, is comparable to the particle hard-core size. This is the typical situation that we are familiar with in elementary phase diagrams of atoms and molecules where van der Waals interactions predominate. Thus, we see the expected pattern of phase behavior. Below the critical temperature, the gas-liquid phase equilibrium occupies the greater part of the low and middle range of densities, above the triple point. The crystal is favored at higher density, and the liquid- and fluid-crystal boundary is nearly vertical, that is at fixed density, reflecting the substantial absence of any energy scale in the problem. The crystal is so tightly packed, and the attractions are so spread out across the system that it is only the repulsive part of the potential
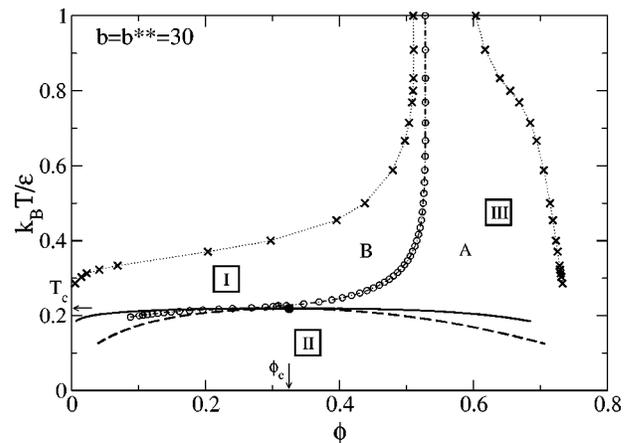

FIG. 6. As in Fig. 3 with $b=30$. For the points A and B see the text. At this b value the glass line passes through the metastable liquid-gas critical point. The labels I, II, and III are chosen by analogy with the proposition of Mushol and Rosenberg [2]. See text for details. The shifted glass line is not represented in this figure and in Fig. 7–10.
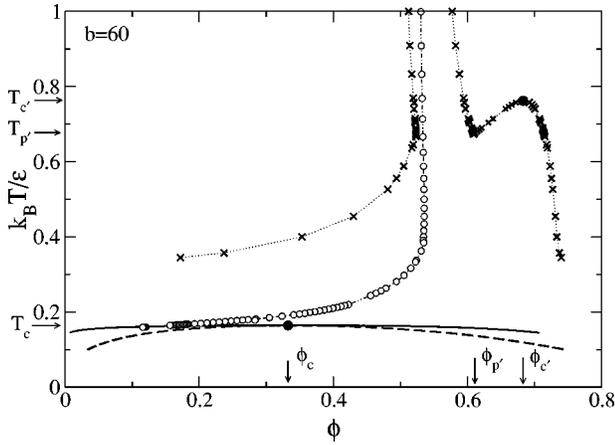
FIG. 7. As in Fig. 3 with $b=60$. The subscripts c' and p' refer now to the critical and triple points of the solid-solid transition.

FIG. 9. Phase diagram for the SW model for $\Delta=0.03$. The crosses represent the solid-fluid phase coexistence and the set of open circles is the glass line. Note the solid-solid coexistence on the high density side of the phase diagram: its critical point is labeled by a filled circle. The position of the liquid-solid-solid triple point is also displayed $(\phi_{p'}, T_{p'})$.

that is fundamental for crystallization. Indeed this is one of the important ideas in traditional liquid state theory that attractions are not relevant to crystallization.

The asymptotic limits of solidification and melting boundaries of this coexistence at high temperatures reflect the hard-sphere limits, respectively, of $\phi \simeq 0.49$ and $\phi \simeq 0.55$, as expected from many simulations and theoretical observations [15,34]. The triple-point temperature is labeled T_p. Within the crystal phase there is also the boundary for the dynamically arrested state (the MCT transition line), again with high-temperature asymptote of $\phi \simeq 0.52$ (circles), the hard-sphere volume fraction for the glass transition predicted by MCT. We recall that MCT underestimates the glass transition packing fraction by about 0.06. To call attention on this shift, we report the true MCT curve (circles) as well as the MCT curve shifted by 0.06 in packing fraction using * as symbol. This boundary is also almost vertical, again reflecting the fact that for wider wells the arrest transition is driven essentially, at high enough temperature by the repulsive part of the potential. Thus, no attractive glass is observed for this range of the potential. It has been shown theoretically [15,14], experimentally [68], and by simulation [16] that on decreasing the range of the attractive potential the fluid-fluid coexist-
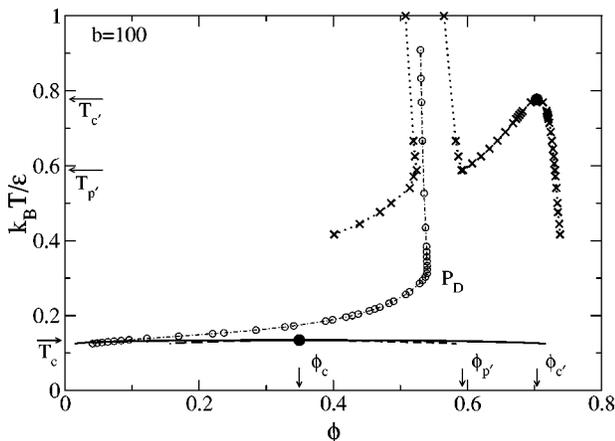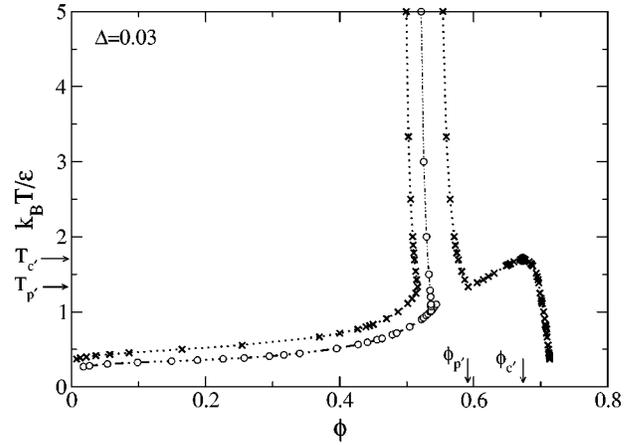

FIG. 8. As in Fig. 3, figures for $b=100$.

ence curve becomes metastable with respect to the fluid-solid one. This means that for short enough potential ranges, the liquid-gas critical point is hidden in a phase separating region. This has two main consequences. The coexistence curve between the fluid and the solid is very broad, implying, for low temperatures, coexistence between a very low density fluid and a high density solid (fcc). Also, the critical point becomes metastable with respect to gas-solid coexistence. We will return to some of the possible implications of all this later in the discussion. We have calculated the particular value of the screening parameter b, at which the critical point becomes metastable with respect to the low density fluid-gas equilibrium, to be $b^*=6.05$, and then presented the phase diagram at that value (see Fig. 4). We note that slightly different values have been previously reported in the literature. Thus, Hagen and Frenkel quote the values $b^*=7.4$ using a Monte Carlo perturbation theory, and the value $b^*=6$ based on GEMC [16]. Their GEMC value is very close to the value we have found. However, a number of other values have also been quoted in the literature. Menderos and Navascues [69] used a density functional approach to determine $b^*=8.25$, while Shukla [28] quotes a much higher value of $b^*=13$. This latter value, in particular, is much higher than previous ones and our value, and considering that it is based on more extensive simulations than previous research this might be a matter of concern. The issues in relation to the accuracy of SCOZA have been addressed for modest values of b in Figs. 1 and 2, where the liquid-gas phase diagrams were shown for $b=1.8$ and $b=6$. However, if we examine Table IV and Fig. 4 of [28], we can readily compare the simulations to the precise predictions from SCOZA for selected values of the vapor and liquid densities for a range of temperatures. For $b^*=6$, we find remarkable agreement between SCOZA and the Shukla gas-liquid equilibria. Also, whilst they are not quoted, we may estimate the critical temperature for differing screening parameters from these simulations, and interpolation of others,

and again conclude that the discrepancy between what we find for b^* and the Shukla result cannot arise due to a difference between the SCOZA and GEMC results for gas-liquid systems. The problem lies in the estimation of the crystal free energy, or entropy, or estimation of the triple point; the other aspect of what we need to know to determine b^*. In [28] the freezing transition location is determined by the so-called one-phase entropic condition [70]. This condition implies that the freezing density is essentially constant and almost unchanged for the range of b values 1.8 to 10 [28]. In fact, in Fig. 4, the phase diagram for $b^*=6.05$, we do see rather significant deviation of the freezing density in the vicinity of the critical temperature from its high-temperature limit. Indeed, comparing the other phase diagrams, Figs. 5–8, we conclude that this variation is intrinsic to the whole short-ranged scenario, since it is the prelude to the splitting of the solid phase into two crystalline phases. The true underlying discrepancy arises because the entropy criterion implies that attractive forces are not important in the regime of crystallization currently under discussion, whereas the perturbation theory implies that they are highly significant. Both approaches are approximations, but it is possible to estimate the errors arising from the perturbation theory by considering the higher-order terms.

Thus, for $b^*=6.05$, (here $k_B T_c^*/\epsilon=0.454$ and $\phi_c^*=0.230$) we can propose to bound the errors in the perturbation theory of the crystal by reporting the ratios of the second- to first-order terms in the perturbation series. In the regime where the low-density fluid and crystal are in equilibrium, we find that the ratio of the second- to first-order terms is approximately 0.0044, whilst the first-order term has an absolute value of 10.4 [71]. If this ratio represents a true estimate of the errors, then the perturbation theory would appear to be quite satisfactory. The curvature of the freezing curve appears genuine and the attendant flattening of the fluid side of the coexistence also appears quite accurate.

In general, by estimating the impact of such errors in perturbation theory, we can estimate the shift of the fluid side of coexistence, and thereby estimate errors. In doing so, we find that the typical error in b^* will be less than 1% from this source. If we accept this means of characterizing the error in perturbation theory, a matter clearly based on the series being well behaved at successive orders, then we might conclude that the value of $b^*=6.05$, in agreement with Frenkel's original calculation, is a good approximation. If this is confirmed, then the calculations reported here for the overall phase diagram are probably amongst the most accurate for modest values of the range parameter, despite the fact that simulation is never used. This is not the primary motivation of our paper, but it would be an interesting way of approaching phase diagrams in future. Despite these optimistic estimates, more careful evaluations are required by different methods to find a truly accurate value.

We should not imply that the value of b^* is of such crucial importance in the overall picture offered here. However, it does provide a useful check between different researchers and methods of approximating the phase behavior in that its accurate estimation requires some satisfactory and simultaneous treatment of gas, liquid, and solid phases.

Finally, we note that ten Wolde and Frenkel have made some interesting comments in relation to the kinetic processes that might be expected in this regime [72].

In Fig. 5 the case $b=7.5$ has been plotted. As noted by a number of authors, the metastable gas-liquid phase equilibrium curve has now flattened considerably, and the low-density fluid-crystal coexistence (on the fluid side) has nearly the same slope. Increase in curvature of the crystal side of the fluid-crystal equilibrium curve is observed, arising from the increased influence of attractions on the crystal. The binodal line and the spinodal line in this case lie completely within the region of fluid-solid phase separation, the triple point has disappeared and the critical point is buried below the flat part of coexistence curve between the low-density fluid and the solid. As we mentioned earlier, this metastable behavior would normally not be observable due to fluctuations, but for colloidal systems, globular proteins and other large particles, we may expect to observe such phenomena. Thus, on quenching such a system, we might expect to see rather a rich pattern of behavior, depending on the density that we quench at, and the depth of the quench. In particular, it is noted that we should be able to see a metastable gas and a liquid; the latter arresting into a glass at sufficiently low temperature, because the glass curve crosses the binodal, and spinodal at a finite temperature. We have earlier alluded to the idea that critical fluctuations can play an important role in the formation of crystals, for example, protein crystals [72]. The present screening parameter regime would exemplify this type of phenomenon since here we have a metastable liquid and gas that are critical (for large particles this should have some observable lifetime). The equilibrium phase diagram exhibits a fluid-crystal coexistence, so we have the possibility of crystal nucleation and growth phenomena in the presence of this metastable critical fluid, and it is this matter that ten Wolde and Frenkel have discussed [72]. However, we also note the point that for this value of the screening parameter, the glass curve has not begun to severely interfere with the gas-solid equilibrium curve as yet and this is an additional advantage in the formation of crystals. This is in distinction to subsequent phase diagrams where the glass curve extends across much of the space.

It is in fact worth reflecting on the shifted, more realistic placement of the glass transition curve (stars). Thus, we see that at high temperature, as expected, from 55% to 58% volume fraction values, we have a crystalline state that is not interrupted by a glass transition. However, as the temperature is lowered, the increased importance of the attraction leads to the glass curve crossing the low density fluid-crystal coexistence region, and beneath this, the crystal may never form without the glass being an alternative long-lived state. This comment is relevant also to the case of $b=6.05$, but for $b=7.5$, the curvature of the solidification curve has increased greatly, so this effect is emphasized. This dramatic interruption of the crystallization scenario will become more and more significant as the range of the potential narrows, and this will be an important theme in our discussion.

Now we turn our investigation to the case of very narrow potential ranges. In Fig. 6 we present the case $b=30$. The two-phase coexistence of fluid and solid now occupies a

much larger portion of the parameter space. The gas-liquid critical point is hidden well below the fluid-solid coexistence line and on the crystal-fluid phase boundary the effects of critical fluctuations will be much less. It is interesting to note that the crystal side of the coexistence curve exhibits a strong deviation towards higher densities. Thus the coexisting solid will be much more dense that in the previous cases, since the strong short-ranged attraction is pulling the particles closer at low temperatures. This phenomenon is the precursor of a solid-solid phase coexistence that in this case is still metastable and lies within the sublimation curve.

The glass transition curve is most interesting. Of course, for $T \to \infty$, the curve asymptotes to the hard-core value. The attractive forces at low temperatures now begin to strongly affect the curve so that it now turns sharply to the left, passing very close to the submerged critical point. Thus, we may tentatively assign $b^{**} = 30.0$ as that value of the screening parameter at which the submerged critical point becomes submerged by the glass, as well as by the crystal-gas curve. The inherent inaccuracies in the MCT estimate, alluded to before, may mean that the b^{**} value may not be very accurate. However, the phenomenon is interesting. It means that the metastable critical fluid is now competing with a glass transition. It will transpire that the nucleation rate of these fluid-crystal equilibria is very low, possibly due to the high interfacial tension and, therefore, it is feasible that one may be able to approach the liquid-gas equilibrium and its nearby glass transition without significant interference of the crystal. The type of slowing that would arise from a combination of critical slowing down and glassy slowing down has not been discussed in the literature previously. It would be an interesting problem. However, the phenomenon discussed here would significantly affect the possibility to form high-quality crystals, perhaps rendering it essentially impossible. Even though the glass may eventually decay in favor of the crystal, this will never lead to high quality crystals. Of course, an alternative view of this situation is that under these conditions it may be possible to make interesting materials that have critical fluctuations frozen into the glassy phase. Protein scientists wish to make good quality crystal; materials scientists often wish to make interesting materials. Our comments are applicable to both situations.

It is interesting also to note that in this case the glass curve passes close to the gas-liquid critical temperature, but then dips and intersects the binodal line below the critical density, passing through the spinodal region. Such a scenario has been found by Verduin and Dhont [4] in experiments on colloidal systems. We should stress that for low densities the glass curve itself may not be reliable, as was discussed in [11]. The situation in relation to this point is, as yet, not settled.

We now discuss the case of extremely narrow wells. It is worth noting that the previous two values of the screening parameters represent the typical range of values accessed by those studying depletion-induced attraction between colloidal particles [5] or globular proteins [1,73]. The next set of phase diagrams (Figs. 7 and 8) represent the limit of these types of interaction and may correspond to cases, such as

grafted coatings on latex particles where we can access much narrower ranges of potentials.

In Figs. 7 and 8, we present the cases $b = 60$ and $b = 100$, respectively. For numerical reasons, it is difficult to extend fluid-solid coexistence curves in the low-density region of the phase diagram. This is evident from the truncation of the phase diagrams, and has no fundamental significance. As already noted in this paper, SCOZA has not been tested with simulations for such narrow ranges of the attractive potential. On the other hand, the main phenomena appear using other methods, so at least these are expected to be reliable. We return to this point at the end of this section.

In both figures we observe similar features. The spinodal line is now buried deep in the sublimation curve as is the critical point. The most striking feature of these phase diagrams is the presence of a solid-solid coexistence. This first-order phase transition was already present for less narrow ranges but there it was metastable (see, for example, the shoulder in the phase diagram for $b = 30$). This phase boundary represents the coexistence of two crystals with the same lattice structure but different lattice spacing and consequently different density [12]. It is terminated by a critical point of the solid-solid coexistence. The origin of this coexistence is interesting. The presence of short-ranged attractive interactions causes competition with the hard-core repulsive interaction. The fact that both have variations that occur on very short-length scales means that the system may be forced to ''choose'' between the attractive-dominated crystal and the repulsive-dominated crystal.

In the low-density crystal region, i.e., $\phi < 0.65$, the crystallization is dominated by entropic effect. In other words the system chooses to optimize the entropy to form an fcc structure. Increasing the density, the particles become closer and at some density they are forced to remain in the attractive shell of their nearest neighbors. When this happens, there is a decrease in energy, which leads to an ''attractive'' crystal. It is the energy that stabilizes the phase. It is indeed clear that such a phenomenon can be present only if the range of the attractive potential is short enough. We may note that an isostructural phase transition has been already discussed theoretically for other kinds of potential characterized by a short-range potential [13] and indeed was also detected by simulation [12,14]. It is almost certainly a genuine phenomenon. Here the isostructural phase transition is present for both $b = 60$ and $b = 100$. Decreasing the range, moves the critical point of the transition to higher density and, indeed, this is also in agreement with the behavior in simulations [12]. It is interesting to note that it is possible to find a triple point T_p at which the two solids and the fluid coexist at the same temperature.

In Figs. 7 and 8 the glass lines have also been plotted. They both tend to the hard-sphere limit for high temperatures, and bend towards low densities with decreasing temperature, as we have seen in the earlier cases. For short enough interaction ranges the glass transition line does not pass close to the critical point. We note that for $b = 100$ the glass curve appears to break into two branches, with an apparent discontinuity at that point marked P_D in the figure. The low-density branch is called attractive glass, while the
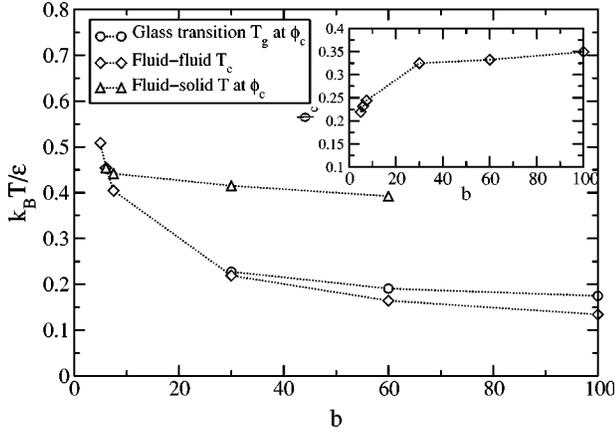
FIG. 10. Critical temperature T_c plotted as a function of the screening parameter b. The glass transition and the solid-fluid coexistence temperature at the critical packing fraction ϕ_c are also displayed. For completeness, in the inset the ϕ_c as a function of b is also shown.

right-hand branch is called repulsive glass. For very short ranges, in other types of attractive potentials, we have located a glass-glass transition, a transition between two different type of glasses originated either by repulsion or by attraction [10]. For the Yukawa fluid such a phenomenon also appears to be present, although it has not yet been investigated in detail [50,51].

Both the results for the Yukawa potential considered here and those for the square-well fluid that we present next for comparison, clearly show that the distinction between the attractive solid and repulsive solid becomes sharper as the range of the potential becomes narrower.

To present in a coherent way, the role of the attractions on the crystal, glass and liquid-gas coexistence line, we show in Fig. 10 the dependence of T_c on b and both the glass transition temperature and the solid-fluid first-order transition temperature at the critical packing fraction ϕ_c. For completeness, the inset shows $\phi_c(b)$.

B. Square-well potential

Finally we discuss a single example for the SW model. By doing so, we wish to make the point that the main phenomena that have been discussed above are independent of the details of the shape of the potential, and are essentially universal. We note, however, that the SW phase diagram is not expected to be so quantitatively accurate as that of the Yukawa potential for reasons discussed in Sec. III.

The SW model was solved as discussed in Sec. II B. We discuss a case where the range of the potential is very narrow, i.e., $\Delta = 0.03$, and the result is presented in Fig. 9. It is clear that the situation is very similar to that for the Yukawa fluid, i.e., a solid-fluid phase coexistence extends from high temperatures (where again it reaches the correct hard-sphere limit) expanding dramatically towards low and high densities for low enough temperatures. An isostructural solid-solid phase transition, with a critical point, is also present in this case. Indeed a limited correspondence between different potentials based on their general characteristics (effective core,

range, and energy scale) has been recently proposed [74], and it is possible that this idea may have more general applicability. We hope to return to this more general concept of corresponding states at a later point [75].

The glass line also has a very similar shape to the Yukawa fluid. As noted above, and in earlier publications, we have a glass-glass transition, terminating in a higher-order glass singularity, the $A3$ transition [10]. We believe that the presence of these two types of glass, the attractive and the repulsive glass, is the disordered analog of the presence of the two types of crystals discussed in some detail above. In this case we may draw also an analogy between the presence of the isostructural critical point and the presence of this MCT singularity A_3 end point at which the two glasses become identical. Also as the well width gets larger, the crystal-crystal critical point vanishes. We believe that the glass-glass analog of this is the A_4 point [10,18].

It is quite reasonable to suppose that for every crystal there should be an analogous glass and for every critical point of such a crystal-crystal equilibrium there should be such an MCT singularity. It will be interesting to explore this idea in future. It has the appeal of a potential general joint classification of equilibrium and glass transitions.

VIII. CONCLUSIONS

We shall use the conclusions section of this paper for two purposes. Thus we shall attempt to sum up the practical conclusions of our calculations, but, at the same time, try to considerably broaden the discussion to make contact with the main experimental situations where they might be useful. So far, we have focused the discussion quite strongly on the narrowly defined consequences of studying a short-ranged hard-core attractive Yukawa potential, so we will begin by summing up that aspect of the discussion.

First, from the technical point of view, we have achieved a certain success combining a good liquid-state method of calculation with the perturbation theory. The resulting hybrid method takes free energies from SCOZA for the gas and liquid states, and from perturbation theory for the crystal. We have indicated, in broad terms, how this overall strategy could be applied to phase diagrams, in general, and how it may be qualified by checking of errors and relating these errors to shifts in the phase boundaries. Given the potential to exploit powerful methods of liquid-state theory and the remarkable success of perturbation theory for the ordered state when one chooses the correct zeroth-order state, this may be a competitive manner in which to proceed for many problems in future.

On the other hand, the methods to determine dynamical arrest (e.g., MCT) are not nearly so developed, despite their relative success in colloidal science. In particular, the absolute values of the density and temperature at which the arrest takes place is not correct. This should not be surprising. Equilibrium theory has had the benefit of many more years of development, and much more effort devoted to bring it to this level of achievement whereas for the dynamical arrest alternative routes or different approaches have been devel-

oped only recently [76]. However, this aspect is quite inconvenient.

As we try to apply this theory to more realistic situations in colloids, materials and biology, we see increasingly this important motif of a competition between the equilibrium Boltzmann view of the matter and the dynamically arrested aspects. So far, these two fields have developed somewhat in independent manner. However from the point of view of these practical topics in nature, there is no distinction, and it is often not the separate behaviors, but the interplay and competition between them that is primary to the scientific issue. This paper is one of the first attempts to make connections between these phenomena, but one can clearly see the limitations. For greater insight into these topics, we will have to address the possibility to both improve systematically the methods of studying arrest transitions, and also their consistency with equilibrium transitions. This must represent one of the important technical challenges in coming years.

From a broader perspective, we have shown that when the range of the potential becomes short in comparison to the core size, the subtle interplay between entropy and energy begins to change its character. The range of densities over which configurational entropy is relevant is much reduced, and one begins to lose the liquid state in favor of crystals or arrested glassy states. The reasons have been discussed at the beginning of the paper. In essence they amount to the fact that to retain the benefits of short-ranged attractions, the particles must not depart too much from their typical interparticle distance, or they are no longer in their mutual attractive well. This loss of freedom of motion and restriction of favorable configurations leads to a lowered configurational entropy. Another way of expressing the same idea is that the short-ranged potential leads to the loss of easy fluctuations that can open the cage of neighboring particles that trap a central particle. The probability of finding such an ''opening'' of the cage is much reduced, and the time during which a particle is localized by its neighbors increases, diverging at the arrest transition to form the ''attractive glass'' that we have discussed. As the range of the potential narrows, the means of egress permitted to the particles is further limited, and the attractive glass becomes more favored. This glass is, therefore, an effective competitor to the liquid and crystalline phases of the system, and this is reflected in the fact that the fluid phase is eventually erased by the glassy phase and the critical point is submerged underneath the curve of arrest transitions. This aspect should not be confused with the equilibrium phase diagram, although it is interesting that there are many parallels between the two.

As we discussed before, when the range of the potential becomes very short, the competition between entropy and energy is responsible for the formation of two distinct crystal phases. Coming from the fluid side, a crystalline phase dominated by repulsion is present. This state arises from the fact that, at such densities, the entropy of a system made of particles free to move only in their own Weigner-Seitz cell of a fcc structure is larger then that of the metastable fluid. We named this phase a repulsive crystal by analogy with the glass. On increasing the density, this crystal becomes unstable and makes a transition to a smaller Weigner-Seitz cell,

so that particles mainly stay within the attractive well. The structure of this phase, that we named attractive crystal, is a more compact fcc crystal that optimizes the free energy by means of reducing the potential energy. The result at this point is that the crystal structure may adopt two different states. The situation is analogous to the case of a gas-liquid phase separation where the gas (low density) phase optimizes the entropy and the liquid (high density) has a much lower energy.

The implications of all this are profound for practical situations. For reasons given earlier, many systems such as colloids, globular proteins, fullerenes, nanoparticles, preceramic particulates, and others have this property of a short-ranged attraction. In all these cases ''precipitation,'' ''gellation,'' ''glassification,'' or solidification are frequently the commonly observed outcomes. In cases where we consciously seek to make such a state, this is satisfactory and it remains only to adjust the potential to have sufficiently short range to obtain the required properties of the solid. However, for cases such as globular proteins, and nanoscale or mesoscale ordered materials with prescribed optical properties, the situation is quite different. Here we seek to make a crystal. In fact, reviewing the phase diagrams in Figs. 5–8, we can see why the crystal is hard to access. If we work to the right side of the glass curve (point marked A in Fig. 6), universally we may expect to fall into the glass state; there is essentially no choice. Since the glass curve moves to low density, this is a serious restriction. However, we may choose to work within the two-phase low-density fluid-crystal coexistence regime, but to the left of the glass curve (point marked B in Fig. 6). The outcome is then a question of kinetic control and will not be completely settled by diagrams, such as, we are drawing. However, we can make some educated comments. Thus, if we work in the two-phase regime of gas solid (B), we may nucleate and grow crystals. Whether the proximity to a metastable critical point is advantageous or not, as discussed by Hagen and Frenkel [16] is not our primary concern here, though this is an interesting proposition. The broader point is that by nucleating to the left of the glass curve one may enter the crystalline region (thus form a macroscopic crystal) by a route not described by the ''adiabatic'' description here, and thereby avoid some of the complications of the glass. This renders the formation of crystal at least feasible, although where the glass curve runs through the two-phase region, it will remain difficult to form truly large high quality crystals. From this region where it is possible to crystallize, one should also exclude the two-phase region, whether it is metastable or not, since the partial (micro-)phase separation, crystallization and glassification, all competing dynamically is unlikely to produce a good crystal also. This leaves only the region bounded to the right by the glass curve, to the bottom by phase separation, and to the top by the gas side of the gas-crystal phase-coexistence as a likely candidate for forming good crystals. This is interesting. It leads us to suppose that for a fixed short range of the potential there is a ''practical crystallization region'' in the temperature-density plane, irrespective of the specific features of the equilibrium phase diagram. However, more importantly, there is also a limited regime of interaction ranges where such a slot is significantly

large enough to be accessed experimentally. We believe that much of the discussion that has taken place in the last few years in the literature in relation to protein crystallization [1,2,77] is almost certainly heading in the correct direction. Thus, Mushol and Rosenberg [2] show in their Fig. 12 the typical situation for a globular protein phase diagram. They exhibit a phase diagram that has (a) two metastable liquid phases in equilibrium, a more and less dilute phase of protein (gas-liquid in our language), (b) a "gellation curve" that we associate with the glass curves in our work, and (c) a fluid-crystal coexistence regime. They name the "good" regime for crystallization zone I, and the others II, and III. We have also essentially partitioned our phase diagram into the same types of zones, and concluded that this gas-crystal region described above by the glass, binodal and gas side of the coexistence boundary (zone I in their language) would be the most favorable for formation of crystals. For the sake of comparison in one of our figures (Fig. 6) that has a range typical of globular proteins, we have marked regions I–III in analogy with Ref. [2].

We would argue that the present work, with its phase diagrams, and discussion of control parameters is the quantitative expression of these ideas that have surfaced in the protein crystal literature. This is potentially encouraging, since it opens the possibility to make more quantitative study of these systems.

However, perhaps the most promising directions involve the study of the current model and underlying ideas in more depth to see what independent kinetic routes exist to the formation of crystals. We have seen how these phase diagrams are indicative of the kinetic behavior, but we believe that there will be much more significant insights as to how to form high quality crystals in these regimes if a deeper under-standing of kinetics is acquired in future. In particular, the glass analogy seems promising as a means to characterize the more confined phase space experienced by these systems. Aging, and kinetic phenomena in general, is an arena that is growing in importance [78–82] and may offer significant advances. The traditional viewpoint of activated processes and simple kinetic processes is without doubt incomplete in the limit where we approach the rather confined phase spaces characterized by approach to a glass transition. The realization that we are in a "glassy" scenario may well assist in development of new theories of kinetics of crystallization more appropriate for such questions.

In any case, one can hardly doubt the high degree of practical significance that kinetic phenomena associated with short-ranged potential systems will have in the coming few years. Given that we discuss a model potential that is only slightly different from those long considered in liquid-state theory, we must be intrigued by the novelty in supposedly simple situations.

[1] R. Piazza, Curr. Opin. Colloid Interface Sci. **5**, 38 (2000).

[2] M. Mushol and F. Rosenberg, J. Chem. Phys. **103**, 10 424 (1995).

[3] H. N. W. Lekkerkerker, W. C. Poon, P. N. Pusey, A. Stroobants, and P. B. Warren, Europhys. Lett. **20**, 559 (1992).

[4] H. Verduin and J. K. G. Dhont, J. Colloid Interface Sci. **172**, 425 (1995).

[5] P. N. Pusey, A. D. Pirie, and W. C. K. Poon, Physica A **201**, 322 (1993); P. N. Pusey, P. N. Segrè, O. P. Behrend, S. P. Meeker, and W. C. K. Poon, *ibid.* **235**, 1 (1996); W. C. K. Poon, Curr. Opin. Colloid Interface Sci. **3**, 593 (1998).

[6] E. Bartsch, V. Frenz, J. Baschnagel, W. Schärtl, and H. Sillescu, J. Chem. Phys. **106**, 3743 (1997); A. Kasper, E. Bartsch, and H. Sillescu, Langmuir **14**, 5004 (1998).

[7] M. H. J. Hagen, E. J. Mejer, G. Mooji, D. Frenkel, and H. N. W. Lekkerkerker, Nature (London) **365**, 425 (1993).

[8] P. G. Debenedetti and F. H. Stillinger, Nature (London) **410**, 259 (2001), and references quoted therein.

[9] F. Sciortino, W. Kob, and P. Tartaglia, Phys. Rev. Lett. **83**, 3214 (1999).

[10] K. A. Dawson, G. Foffi, M. Fuchs, W. Götze, F. Sciortino, M. Sperl, P. Tartaglia, Th. Voigtmann, and E. Zaccarelli, Phys. Rev. E **63**, 011401 (2001).

[11] E. Zaccarelli, G. Foffi, P. Tartaglia, F. Sciortino, and K. A. Dawson, Phys. Rev. E **63**, 031501 (2001).

[12] P. Bolhuis and D. Frenkel, Phys. Rev. Lett. **72**, 2211 (1994); P. Bolhuis, M. Hagen, and D. Frenkel, Phys. Rev. E **50**, 4880 (1994).

[13] C. F. Tejero, A. Daanoun, H. N. W. Lekkerkerker, and M. Baus, Phys. Rev. Lett. **73**, 752 (1994); Phys. Rev. E **51**, 558 (1995).

[14] M. Dijkstra, J. M. Brader, and R. Evans, J. Phys.: Condens. Matter **11**, 10 079 (1999).

[15] A. P. Gast, W. B. Russell, and C. K. Hall, J. Colloid Interface Sci. **96**, 1977 (1983); **109**, 161 (1986).

[16] M. Hagen and D. Frenkel, J. Chem. Phys. **101**, 4093 (1994).

[17] R. Evans (private communication).

[18] W. Götze, in *Liquids, Freezing and Glass Transition*, edited by J. P. Hansen, D. Levesque, and J. Zinn-Justin (North-Holland, Amsterdam, 1991), p. 287.

[19] J. Bergenholtz and M. Fuchs, Phys. Rev. E **59**, 5706 (1999).

[20] L. Fabbian, W. Goetze, F. Sciortino, P. Tartaglia, and F. Thiery, Phys. Rev. E **59**, R1347 (1999).

[21] D. Pini, G. Stell, and N. B. Wilding, Mol. Phys. **95**, 483 (1998).

[22] C. Caccamo, G. Pellicane, D. Costa, D. Pini, and G. Stell, Phys. Rev. E **60**, 5533 (1999).

[23] R. Sear, J. Chem. Phys. **111**, 4800 (1999).

[24] D. Pini, G. Stell, and N. B. Wilding, J. Chem. Phys. **115**, 2702 (2001).

[25] N. F. Carnahan and K. E. Sterling, J. Chem. Phys. **51**, 635 (1969).

[26] E. Waisman, Mol. Phys. **25**, 45 (1973).

[27] J. P. Hansen and I. R. McDonald, *Theory of Simple Liquids* (Academic Press, London, 1986).

[28] K. P. Shukla, J. Chem. Phys. **112**, 10 538 (2000).

[29] C. Rascon, L. Mederos, and G. Navascues, Phys. Rev. Lett. **77**, 2249 (1996).

[30] J. K. Percus and G. J. Yevick, Phys. Rev. **110**, 1 (1958).

[31] R. J. Baxter, Aust. J. Phys. **21**, 563 (1968).

[32] J. A. Barker and D. J. Henderson, J. Chem. Phys. **47**, 2856 (1967).

[33] W. H. Press, S. A. Teukolsky, W. T. Vetterling, and B. P. Flannery, *Numerical Recipes in C*, 2nd ed. (Cambridge University Press, Cambridge, 1993).

[34] B. J. Alder, W. G. Hoover, and D. A. Young, J. Chem. Phys. **49**, 3688 (1968).

[35] U. Gasser, E. Weeks, A. Schofield, P. N. Pussey, and D. A. Weitz, Science **292**, 258 (2001).

[36] S. Auer and D. Frenkel, Nature (London) **409**, 1020 (2001).

[37] S. Pronk and D. Frenkel, J. Chem. Phys. **110**, 4589 (1999).

[38] K. R. Hall, J. Chem. Phys. **57**, 2252 (1971).

[39] D. Frenkel (private communication).

[40] J. M. Kincaid and J. J. Weis, Mol. Phys. **34**, 931 (1977).

[41] L. Verlet and J. J. Weis, Phys. Rev. A **5**, 939 (1972).

[42] P. N. Pusey, in *Liquids, Freezing and Glass Transition* (Ref. [18]), p. 763.

[43] W. van Megen and S. M. Underwood, Phys. Rev. Lett. **70**, 2766 (1993); Phys. Rev. E **49**, 4206 (1994).

[44] W. Götze, J. Phys.: Condens. Matter **11**, A1 (1999).

[45] R. J. Baxter, J. Chem. Phys. **49**, 2770 (1968).

[46] G. Stell, J. Stat. Phys. **63**, 1203 (1991).

[47] Y. C. Liu, S. H. Chen, and J. S. Huang, Phys. Rev. E **54**, 1698 (1996).

[48] R. Piazza, V. Peyre, and V. Degiorgio, Phys. Rev. E **58**, R2733 (1998).

[49] G. Foffi, E. Zaccarelli, F. Sciortino, P. Tartaglia, and K. A. Dawson, J. Stat. Phys. **100**, 363 (2000).

[50] J. Bergenholtz and M. Fuchs (private communication).

[51] K. A. Dawson, G. Foffi, G. D. McCullagh, F. Sciortino, P. Tartaglia, and E. Zaccarelli, J. Phys.: Condens. Matter (to be published).

[52] M. C. Grant and W. B. Russel, Phys. Rev. E **47**, 2606 (1993).

[53] A. Meller, T. Gisler, D. A. Weitz, and J. Stavans, Langmuir **15**, 1918 (1999).

[54] W. Poon (private communication).

[55] S. Neser, C. Bechinger, P. Leiderer, and T. Palberg, Phys. Rev. Lett. **79**, 2348 (1997).

[56] W. Schaertl and C. Roos, Phys. Rev. E **60**, 2020 (1999).

[57] S. H. Behrens, M. Borkovec, and P. Schurtenberger, Langmuir **14**, 1951 (1998).

[58] S. Henderson, S. Mitchell, and P. Bartlett, Colloid Surf., A **190**, 81 (2001).

[59] J. R. Weeks, J. S. van Duijneveldt, and B. Vincent, J. Phys.: Condens. Matter **12**, 9599 (2000).

[60] S. Meyer, P. Levitz, and A. Delville, J. Phys. Chem. B **105**, 9595 (2001); I. Grillo, P. Levitz, and T. Zemb, Eur. Phys. J E **5**, 377 (2001).

[61] F. Mallamace, P. Gambadauro, N. Micali, P. Tartaglia, C. Liao, and S. H. Chen, Phys. Rev. Lett. **84**, 5431 (2000).

[62] W. Götze and L. Sjögren, J. Phys.: Condens. Matter **1**, 4203 (1989).

[63] H. E. Stanley, *Introduction to Phase Transitions and Critical Phenomena* (Oxford University Press, Oxford, 1997).

[64] J. D. Gunton and M. Droz, *Introduction to the Dynamics of Metastable and Unstable Phases*, edited by J. Zittartz, Lecture Notes in Physics Vol. 183 (Springer-Verlag, Berlin, 1983).

[65] J. D. Gunton, M. San Miguel, and P. S. Sahni, in *Phase Transition and Critical Phenomena*, edited by D. Domb and J. L. Lebowitz (Academic, London, 1983), Vol. 8.

[66] P. Schurtenberger, R. A. Chamberlin, G. M. Thurston, J. A. Thomson, and G. B. Benedek, Phys. Rev. Lett. **63**, 2064 (1989); B. M. Fine, J. Pande, A. Lomakin, O. O. Ogun, and G. B. Benedek, *ibid.* **74**, 198 (1995).

[67] M. E. Fisher, Phys. Rev. Lett. **57**, 1911 (1986).

[68] S. M. Ilett, A. Orrock, W. C. K. Poon, P. N. Pusey, Phys. Rev. E **51**, 1344 (1995); W. C. K. Poon, A. D. Pirie, and P. N. Pusey, Faraday Discuss. **101**, 65 (1995); W. C. K. Poon, Phys. Rev. E **55**, 3762 (1995).

[69] L. Menderos and G. Navascues, J. Chem. Phys. **101**, 9841 (1994).

[70] P. V. Giaquinta, Physica A **187**, 145 (1992).

[71] We estimated this ratio for different values of the screening parameter and for different temperatures. The largest value is found to be less than 0.025, but the typical value is much smaller. It decreases for high density. This agrees with Stell and Penrose comment that such an expansion should be exact at the first order in the close packing limit [83].

[72] P. R. ten Wolde and D. Frenkel, Science **277**, 1975 (1997).

[73] A. Tardieu, A. Le Verge, M. Malfois, F. Bonnete, S. Finet, M. Ries-Kautt, and L. Belloni, J. Cryst. Growth **196**, 193 (1999).

[74] M. G. Noro and D. Frenkel, J. Chem. Phys. **113**, 2941 (2000).

[75] G. Foffi, E. Zaccarelli, F. Sciortino, P. Tartaglia, and K. A. Dawson (unpublished).

[76] E. Zaccarelli, G. Foffi, F. Sciortino, P. Tartaglia, and K. A. Dawson, Europhys. Lett. **55**, 139 (2001); E. Zaccarelli, G. Foffi, P. De Gregorio, F. Sciortino, P. Tartaglia, and K. A. Dawson, J. Phys.: Condens. Matter (to be published).

[77] A. George and W. W. Wilson, Acta Crystallogr., Sect. D: Biol. Crystallogr. **D50**, 361 (1994).

[78] J-P. Bouchad, L. Cugliandolo, J. Kurchan, and M. Mezard, Physica A **226**, 243 (1996).

[79] W. Kob and J.-L. Barrat, Phys. Rev. Lett. **78**, 4581 (1997); G. Parisi, *ibid.* **79**, 3660 (1997).

[80] A. Latz, J. Phys.: Condens. Matter **12**, 6353 (2000); e-print cond-mat/0106086.

[81] P. De Gregorio, F. Sciortino, P. Tartaglia, E. Zaccarelli, and K. A. Dawson, Physica A (to be published), e-print cond-mat/0111018.

[82] F. Sciortino and P. Tartaglia, J. Phys.: Condens. Matter **13**, 9127 (2001).

[83] G. Stell and O. Penrose, Phys. Rev. Lett. **52**, 85 (1984).